iScience

CellPress
OPEN ACCESS

Article

SIRT3 differentially regulates lysine benzoylation from SIRT2 in mammalian cells

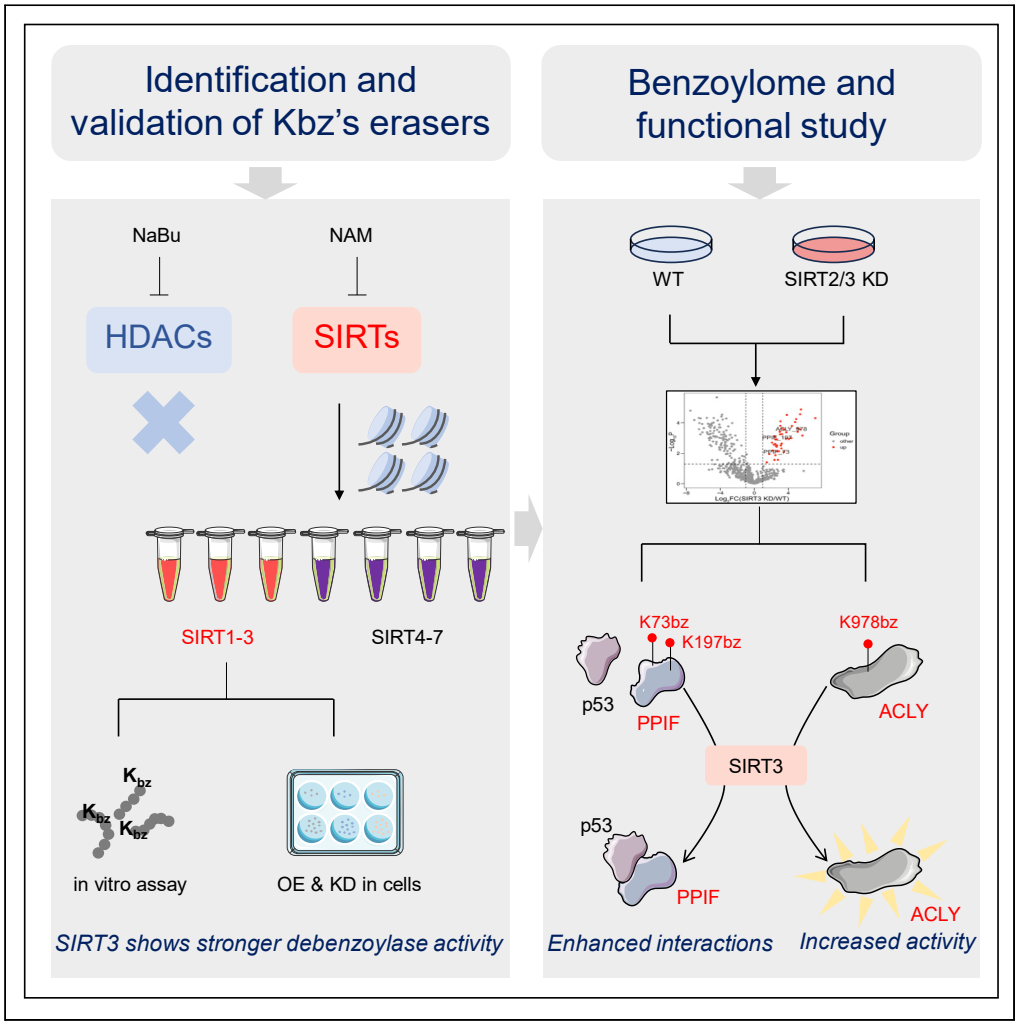

Panpan Peng, Ying Lu, Xuelian Ren, ..., Ruilong Liu, Xiaohan Song, He Huang

hhuang@simm.ac.cn

Highlights

SIRT3 functions as a debenzoylase both *in vitro* and in mammalian cells

SIRT3 and SIRT2 differentially regulate the benzoylome in HepG2 cells

SIRT3-mediated K73bz and K197bz of PPIF weaken its interaction with p53

SIRT3-regulated K978bz of ACLY inhibits its enzymatic activity

Peng et al., iScience 27, 111176
November 15, 2024
https://doi.org/10.1016/j.isci.2024.111176

iScience

CellPress
OPEN ACCESS

Article

SIRT3 differentially regulates lysine benzoylation from SIRT2 in mammalian cells

Panpan Peng,[1,2] Ying Lu,[3] Xuelian Ren,[1,2] Cong Yan,[2] Xinlong Guo,[2] Ruilong Liu,[2] Xiaohan Song,[1,2] and He Huang[1,2,3,4,*]

SUMMARY

Lysine benzoylation (Kbz), a new type of protein post-translational modification (PTM) we discovered, has garnered significant attention. While we initially identified SIRT2 as a debenzoylase in mammalian cells, recent findings suggest its exclusivity may be questioned. However, other debenzoylases in mammalian cells remain underexplored. Here, our study reveals SIRT3 as an additional debenzoylase. Through quantitative analysis, we identified 1,075 Kbz sites in mammalian cells, with 44 specifically mediated by SIRT3 and 66 influenced by SIRT2. Notably, SIRT3 and SIRT2 regulate distinct Kbz substrates, indicating involvement in different cellular processes. Functional investigations demonstrated SIRT3's regulation of benzoylated protein peptidyl-prolyl *cis*-trans isomerase F (PPIF), where K73bz and K197bz markedly diminished interactions with the tumor suppressor p53. Additionally, K978bz on ATP-citrate lyase (ACLY) notably inhibited its enzymatic activity. This study not only identifies a debenzoylase and its Kbz substrates but also enhances our understanding of Kbz's biological functions.

INTRODUCTION

Protein post-translational modifications (PTMs) play pivotal roles in numerous cellular functions. They impact the spatial conformation, activity, and interactions of proteins, thus contributing to the regulation of various physiological and pathological processes, including gene transcription, cellular metabolism, and cancer.[1–3] In the last decade, several new types of acylations have been identified, such as lysine β-hydroxybutyrylation (Kbhb),[2] benzoylation (Kbz),[4] and lactylation (Kla).[5] These PTMs assume critical regulatory roles in diverse cellular pathways, thereby enhancing our comprehension of the intricate biological processes in organisms.

Kbz was discovered by us and has received increasing attention due to its unique structural and chemical characteristics compared to other known lysine acylations.[4] Its distinctive feature lies in the presence of an aromatic ring moiety at its terminal, rendering it larger in size and more hydrophobic than other short-chain fatty acylations, thus suggesting its unique cellular functions and landscape of the regulatory elements. Dysregulation of PTMs has been demonstrated to contribute to numerous diseases.[6–8] Therefore, identification of the regulatory enzymes and corresponding substrates of Kbz is critical to comprehend its role in physiology and pathology.

The deposition and removal of PTMs are dynamically regulated by a variety of enzymes, with "writers" attaching chemical groups to lysine residues and "erasers" responsible for removing these modifications. For example, the extensively studied lysine acetylation (Kac) undergoes a dynamic equilibrium between histone acetyltransferases (HATs) and deacetylases (HDACs), as is the case with many other acylations. HDACs consist of 18 members categorized into four classes: class I Rpd3-like proteins (HDAC1–3 and HDAC8), class II Hda1-like proteins (HDAC4–7, HDAC9, and HDAC10), class III Sir2-like proteins (SIRT1–7), and class IV proteins HDAC11.[9] Classes I, II, and IV HDACs are zinc-dependent, while class III HDACs use NAD^+ to generate nicotinamide (NAM) and the metabolite 2′-*O*-acetyl-ADP-ribose during deacetylation.[10]

In our previous study, we carried out an *in vitro* screening using a H2BK5bz peptide as the substrate, revealing that SIRT2 could remove histone Kbz.[4,11] However, certain indications suggest that SIRT2 may not be the sole debenzoylase in mammalian cells. For example, overexpression of SIRT2 in 293T cells predominantly affected Kbz levels on H2B, with no obvious change observed on H4.[4] Theoretically, *in vitro* screening results obtained using a single peptide as the substrate may not provide valuable clues if debenzoylases exhibit sequence preference for substrates. Therefore, screening for debenzoylases using the substrates bearing sequence diversity and validating their debenzoylase activities in mammalian cells are essential to explore the potential functions of Kbz. Moreover, if additional debenzoylases are identified, what specific substrates can they and SIRT2 catalyze in mammalian cells? Are the Kbz sites mediated by these debenzoylases widely distributed across the global proteome? What biological pathways are impacted by the debenzoylase-mediated Kbz substrates? Addressing these questions is crucial for revealing the potential roles of Kbz in diverse cellular processes.

[1]School of Pharmaceutical Science and Technology, Hangzhou Institute for Advanced Study, University of Chinese Academy of Sciences, Hangzhou, China
[2]State Key Laboratory of Chemical Biology, Shanghai Institute of Materia Medica, Chinese Academy of Sciences, Shanghai, China
[3]School of Chinese Materia Medica, Nanjing University of Chinese Medicine, Nanjing, China
[4]Lead contact
*Correspondence: hhuang@simm.ac.cn
https://doi.org/10.1016/j.isci.2024.111176

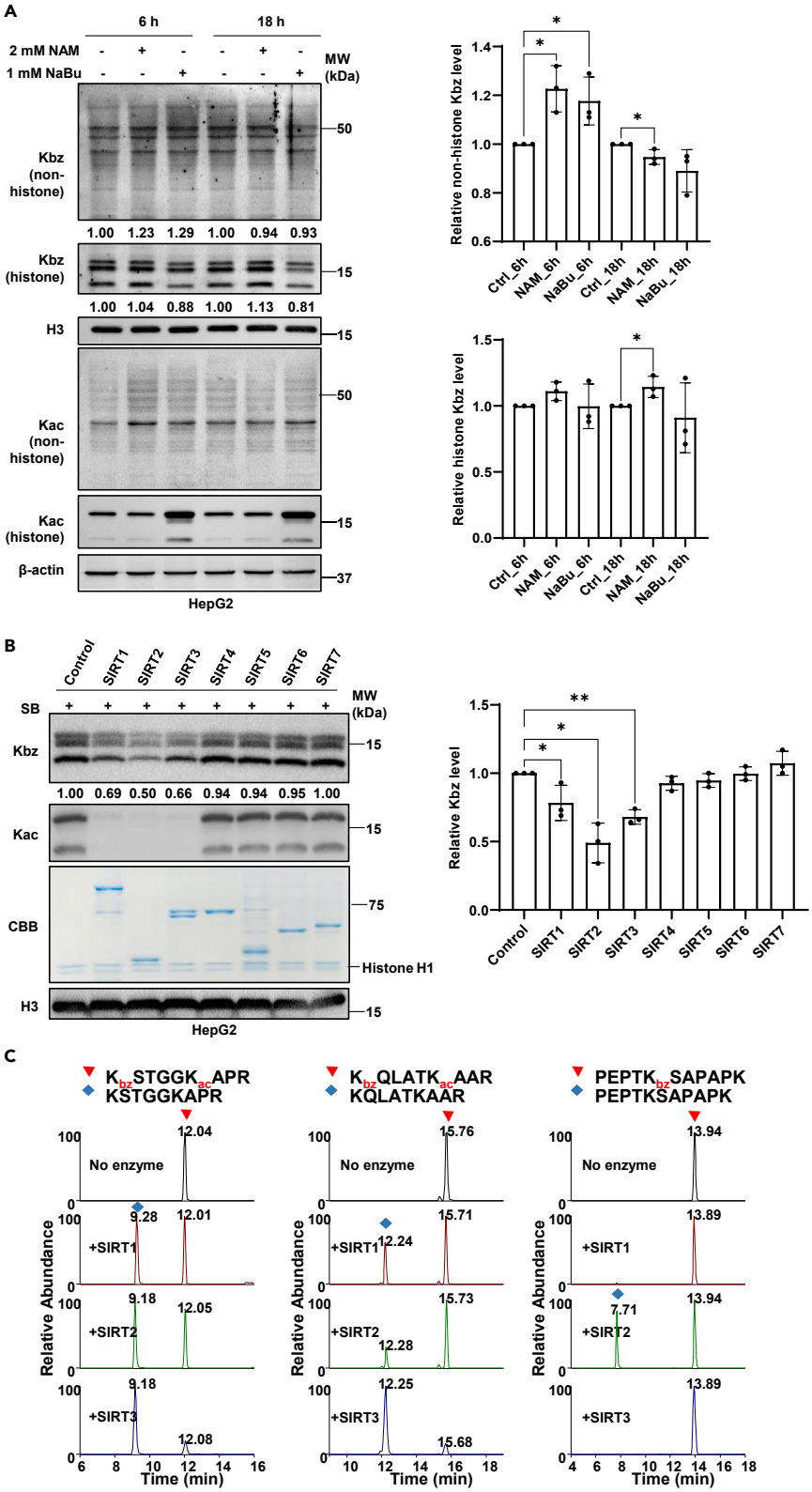
A
6 h
18 h
2 mM NAM
1 mM NaBu
MW (kDa)
Kbz (non-histone)
1.00 1.23 1.29 1.00 0.94 0.93
Kbz (histone)
1.00 1.04 0.88 1.00 1.13 0.81
H3
Kac (non-histone)
Kac (histone)
β-actin
HepG2
Relative non-histone Kbz level
Relative histone Kbz level
Ctrl_6h
NAM_6h
NaBu_6h
Ctrl_18h
NAM_18h
NaBu_18h
B
Control
SIRT1
SIRT2
SIRT3
SIRT4
SIRT5
SIRT6
SIRT7
SB
Kbz
1.00 0.69 0.50 0.66 0.94 0.94 0.95 1.00
Kac
CBB
Histone H1
H3
HepG2
Relative Kbz level
C
K$_{bz}$STGGK$_{ac}$APR
KSTGGKAPR
K$_{bz}$QLATK$_{ac}$AAR
KQLATKAAR
PEPTK$_{bz}$SAPAPK
PEPTKSAPAPK
No enzyme
+SIRT1
+SIRT2
+SIRT3
12.04
9.28
12.01
9.18
12.05
9.18
12.08
15.76
12.24
15.71
12.28
15.73
12.25
15.68
13.94
7.71
13.89
13.94
13.89
Relative Abundance
Time (min)

Figure 1. SIRT1 and SIRT3 remove histone Kbz *in vitro*

(A) Upregulated protein Kbz levels in response to pharmacological inhibition of SIRTs. HepG2 cells were treated with 10 mM SB for 24 h. Simultaneously, the cells were treated with 2 mM NAM or 1 mM NaBu for 6 h or 18 h. Kbz and Kac levels were assessed by western blot using the indicated antibodies. Data are represented as mean ± SEM. $n = 3$, biologically independent sample. p value was assessed by one-sided Student's t test. $^{*}p < 0.05$; $^{**}p < 0.01$.

(B) SIRT1-3 removal of histone lysine benzoylation *in vitro*. Histones were extracted from HepG2 cells treated with 10 mM sodium benzoate for 24 h and then incubated with or without SIRT1-7. Kbz and Kac levels were measured by western blot using the indicated antibodies, with H3 serving as a loading control. Data are represented as mean ± SEM. $n = 3$, biologically independent sample. p value was assessed by one-sided Student's t test. $^{*}p < 0.05$; $^{**}p < 0.01$.

(C) SIRT1-3 removal of Kbz from synthetic Kbz peptides (PEPTKbzSAPAPK, KbzSTGGKacAPR, and KbzQLATKacAAR) in the *in vitro* debenzoylation assay. The peptides were analyzed by HPLC-MS/MS.

In this study, using core histones extracted from benzoate-treated mammalian cells as substrates, we performed an *in vitro* screening and identified SIRT1 and SIRT3, in addition to SIRT2, as enzymes capable of removing Kbz. Validation in mammalian cells affirmed the debenzoylase activities of SIRT1 and SIRT3, with SIRT3 potentially assuming a more significant regulatory role in debenzoylation. Furthermore, we carried out a quantitative analysis of the benzoylome, identifying 1075 Kbz sites throughout the global proteome in HepG2 cells, of which 44 were specifically mediated by SIRT3 and 66 by SIRT2. Bioinformatics analysis revealed that benzoylated proteins regulated by different debenzoylase are implicated in distinct biological processes. Functional studies corroborated that the benzoylation of peptidyl-prolyl *cis*-trans isomerase F (PPIF) at K73 and K197 and ATP-citrate lyase (ACLY) at K978 impeded their interactions with p53 and enzymatic activity, respectively.

In summary, this study not only identifies SIRT3 as an additional debenzoylase, both *in vitro* and within mammalian cells, but also reveals the specific regulation of Kbz substrates by SIRT3 and SIRT2. Additionally, our discovery highlights the impact of SIRT3 on the function of specific non-histone proteins through the regulation of Kbz modification. This sheds light on the molecular functions associated with Kbz, thereby expanding our insights into the potential biological roles governed by the Kbz pathway.

RESULTS

SIRT1 and SIRT3 exhibit histone Kbz removal *in vitro*

To comprehensively investigate the regulation of global Kbz by SIRTs and HDACs, we treated 293T cells and HepG2 cells with the pan-sirtuin inhibitor NAM and the pan-HDAC inhibitor sodium butyrate (NaBu), respectively. The cells were treated with 2 mM NAM or 1 mM NaBu during the last 6 h or 18 h before collection. Western blotting (WB) analysis using anti-pan Kbz and anti-pan Kac antibodies showed that while NaBu significantly increased histone Kac levels in 293T and HepG2 cells, the Kbz level remained stable or even decreased, except at 6 h in HepG2 cell. In contrast, NAM treatment for 6 h enhanced non-histone Kbz levels in HepG2 cells and upregulated histone Kbz levels in HepG2 cells and global Kbz levels in 293T cells after 18 h, with minimal effect on Kac signals (Figures 1A and S1A). These results suggest that SIRTs, rather than HDACs, play a pivotal role in removing Kbz across the global proteome in mammalian cells.

Given the observed elevation of global Kbz levels in mammalian cells upon treatment with the pan-sirtuin inhibitor NAM, we sought to assess the debenzoylase activity of individual sirtuin member. Current evidence suggests that enzymes regulating PTMs often display preferences and selectivity for the flanking sequences of target substrate sites, leading to distinct downstream signals.[12–15] To circumvent potential biases associated with using a single peptide as the substrate for screening, we employed core histones as the substrate for our *in vitro* assay. To ensure a relatively high level of Kbz on the histone substrates, we pre-treated HepG2 cells with 10 mM sodium benzoate (SB) for 24 h before extracting histones. Subsequently, the histone substrates were incubated with purified recombinant sirtuin proteins SIRT1-7, and WB analysis was performed to detect histone Kbz and Kac levels post-incubation, with the latter serving as a positive control to validate the activities of SIRT1-7 (Figures 1B and S1B). The result revealed that both SIRT1 and SIRT3 could reduce histone Kbz levels *in vitro*, albeit to a lesser extent than SIRT2 (Figure 1B).

To further confirm the debenzoylase activities of SIRT1-3, an additional *in vitro* debenzoylation assay was performed using three synthetic Kbz peptides as substrates: H3K9bz (KbzSTGGKacAPR), H3K18bz (KbzQLATKacAAR), and H2BK5bz (PEPTKbzSAPAPK). Consistent with our prior study, only SIRT2 removed the Kbz on H2BK5. However, both SIRT1 and SIRT3 exhibited the ability to remove the Kbz on H3K9 and H3K18, with equal or stronger catalytic activity compared to SIRT2 (Figure 1C).

Collectively, these data indicated that, in addition to SIRT2, SIRT1 and SIRT3 also possess debenzoylase activity *in vitro*. Notably, they exhibit substrate sequence preferences, suggesting potential differentially regulation of Kbz and, consequently, diverse biological consequences.

SIRT1 and SIRT3 regulate protein Kbz in mammalian cells

To investigate the potential modulation of histone Kbz by SIRT1 and SIRT3 in mammalian cells, we introduced FLAG or HA-tagged SIRT1-3 into 293T and HepG2 cells, respectively. After 48 h of transfection, cells were harvested for WB analysis to assess the impact of SIRT1-3 overexpression on global Kbz levels. The results indicated that overexpression of SIRT1-3 resulted in varying degrees of reduction in histone or non-histone Kbz levels in both 293T and HepG2 cells, except for SIRT2 which did not cause a significant downregulation of non-histone Kbz in 293T cells. Overall, SIRT3 demonstrated a slightly stronger ability to remove Kbz compared to SIRT1 (Figures 2A and S2A).

To further validate the debenzoylase activity of SIRT1 and SIRT3 in mammalian cells, we investigated the changes in Kbz levels following knockdown of SIRT1 or SIRT3. Lentiviral infection was employed to stably decrease SIRT1/2/3 expression in 293T and HepG2 cells using short hairpin RNA (shRNA). The efficiency of SIRT1-3 deletion and Kbz levels on both histones and non-histone proteins were assessed through WB

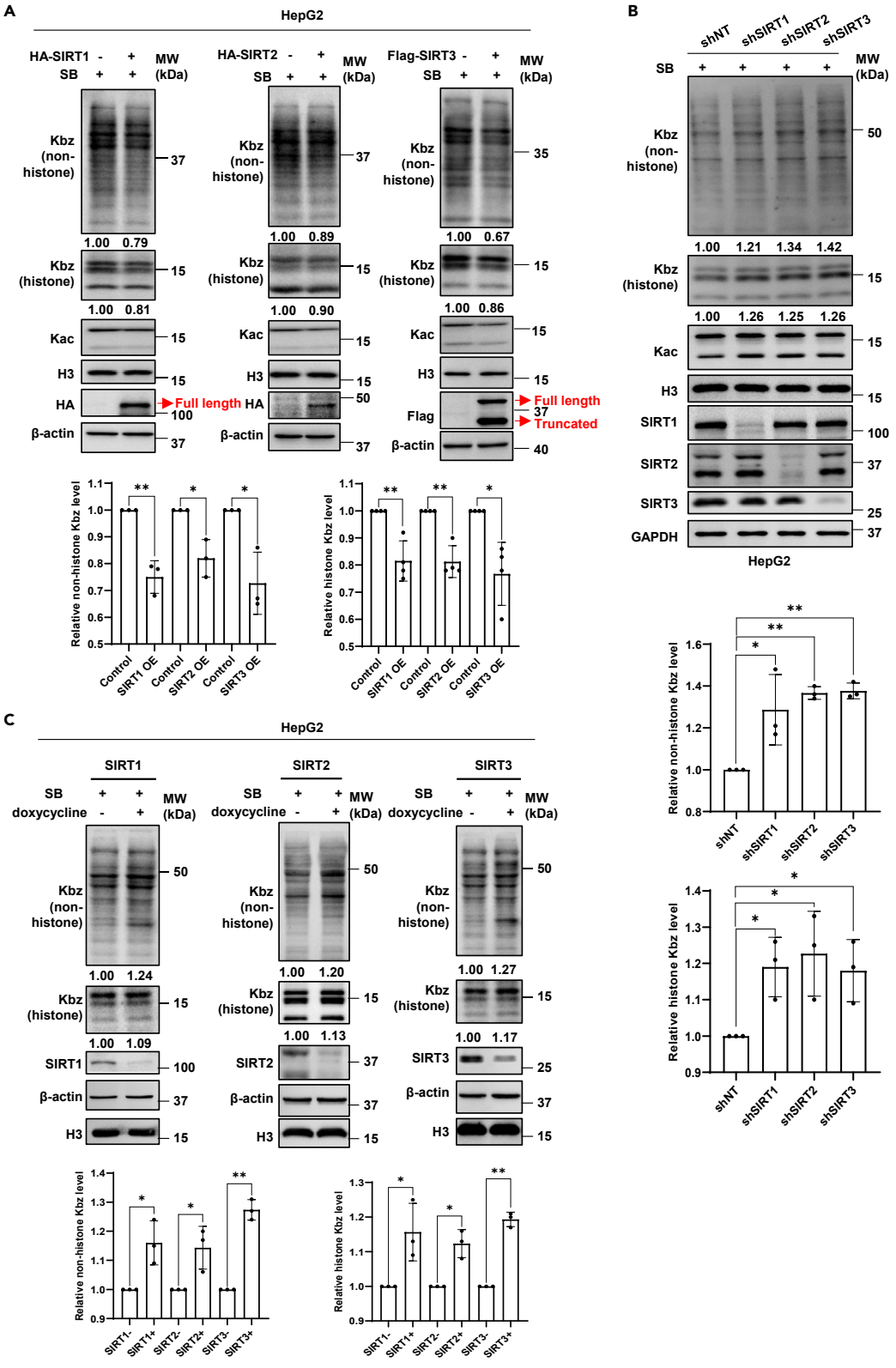
A
HepG2
HA-SIRT1
SB
MW (kDa)
Kbz (non-histone)
Kbz (histone)
Kac
H3
HA
Full length HA
β-actin
HA-SIRT2
Flag-SIRT3
Flag
Full length
Truncated
Relative non-histone Kbz level
Relative histone Kbz level
Control
SIRT1 OE
SIRT2 OE
SIRT3 OE
B
shNT
shSIRT1
shSIRT2
shSIRT3
SIRT1
SIRT2
SIRT3
GAPDH
HepG2
C
HepG2
SIRT1
SIRT2
SIRT3
doxycycline
Relative non-histone Kbz level
Relative histone Kbz level
SIRT1-
SIRT1+
SIRT2-
SIRT2+
SIRT3-
SIRT3+

Figure 2. SIRT1 and SIRT3 modulate protein Kbz in HepG2 cells

(A) Diminished global Kbz levels upon overexpression of SIRT1-3. HA-tagged SIRT1-3 was transfected into HepG2 cells. Twenty-four hours post-transfection, cells were treated with 10 mM SB for 24 h. Whole-cell lysates were subjected to western blot analysis using the indicated antibodies. Data are represented as mean ± SEM. $n = 3$ or 4, biologically independent sample. p value was assessed by one-sided Student's t test. *$p < 0.05$; **$p < 0.01$.

(B) Enhanced protein Kbz levels upon depletion of SIRT1-3. Stable SIRT1-3 knockdown HepG2 cells were treated with 5 mM SB for 24 h. Whole-cell lysates were analyzed by western blot with indicated antibodies. Data are represented as mean ± SEM. $n = 3$, biologically independent sample. p value was assessed by one-sided Student's t test. *$p < 0.05$; **$p < 0.01$.

(C) Increased Kbz levels after SIRT1-3 inducible knockdown. Stably transfected cells with inducible knockdown of SIRT1-3 in HepG2 were successfully generated using the inducible knockdown system. To achieve specific target gene knockdown, the cells were treated with 1 μg/mL doxycycline for 72 h, with a fresh doxycycline solution changed every 24 h. Concurrently, the cells were treated with 10 mM SB for 24 h. Whole-cell lysates were subjected to western blot analysis with the indicated antibodies. Data are represented as mean ± SEM. $n = 3$, biologically independent sample. p value was assessed by one-sided Student's t test. *$p < 0.05$; **$p < 0.01$.

analysis. The results showed a significant increase in global Kbz level in HepG2 cells following near-complete deletion of SIRT1-3 (Figure 2B). Similarly, in 293T cells, knocking down SIRT1-3 also upregulated global Kbz levels to varying degrees (Figure S2B). Notably, consistent with the overexpression assay, SIRT3 exhibited stronger debenzoylase activity compared to SIRT1 (Figures 2A, 2B, S2A, and S2B). The presence of Kbz on non-histone proteins in eukaryotic cells suggests that Kbz may influence various biological processes through non-epigenetic mechanisms. Together, these results affirmed that SIRT1 and SIRT3 play regulatory roles in modulating Kbz in mammalian cells.

Since Kbz is regulated by multiple debenzoylases, stable knockdown of a single debenzoylase may lead to a new homeostasis in cells, introducing genetic compensation that could impact results. This phenomenon has been observed in a recent study where unexpected outcomes were noted upon the deletion of specific HAT or HDAC gene in yeast cells.[11] To mitigate the potential effects of genetic compensation by isozymes, we established an inducible knockdown system. This system allows for the depletion of the target gene only when cells are induced by exogenous doxycycline. The statistical analysis revealed that inducible knockdown of SIRT1-3 in HepG2 cells elevated global Kbz levels (Figure 2C). Similarly, in 293T cells, inducible knockdown of SIRT1 and SIRT3 upregulated global Kbz levels, whereas knockdown of SIRT2 only significantly increased histone Kbz levels (Figure S2C). Analyzing the results of shRNA and induced knockdown of SIRT1-3, we observed distinct patterns in Kbz regulation by SIRT1-3. In summary, SIRT3 exhibited more prominent debenzoylase activity than SIRT1 (Figures 2A–2C and S2A–S2C).

Identification of SIRT2- and SITR3-regulated Kbz substrates

Given the pivotal role of SIRT3 in Kbz regulation, we sought to elucidate the Kbz sites regulated by SIRT3 and the previously reported SIRT2. To achieve this, we performed a label-free quantitative benzoylome analysis following inducible knockdown of SIRT2 and SIRT3. The experiments were carried out in triplicates (Figure 3A). Briefly, total proteins were extracted from HepG2 cells after 10 mM SB treatment for 24 h, in response to 1 μg/mL doxycycline or not for 48 h. These proteins were separately digested into peptides by trypsin, and benzoylated peptides were enriched using anti-pan Kbz antibody, followed by High Performance Liquid Chromatography-Tandem Mass Spectrometry (HPLC-MS/MS) analysis. In total, we identified 1,075 Kbz sites in 556 proteins (Tables S1 and S4), with 66 and 44 specifically modulated by SIRT2 and SIRT3, respectively (fold change > 2, $p < 0.05$, Tables S2 and S3). Interestingly, only three sites were co-regulated by both enzymes (Figures 3B and 3C). Motif analysis of the benzoylated peptides uncovered distinct sequence patterns in substrates differentially influenced by SIRT2 and SIRT3 (Figure S3). To further understand the biological differences between the two debenzoylases, we performed functional and pathway enrichment analysis. Gene Ontology (GO) analysis revealed significant differences in the biological process (BP), cellular component (CC) and molecular function (MF) regulated by SIRT2 and SIRT3 (Figure 3D). Kyoto Encyclopedia of Genes and Genomes (KEGG) results demonstrated that SIRT2-regulated Kbz proteins were mainly involved in protein processing in endoplasmic reticulum, carbon metabolism and viral carcinogenesis, while SIRT3-mediated Kbz proteins were primarily enriched in carbon metabolism, glycolysis/gluconeogenesis, and biosynthesis of amino acid (Figure 3E). In conclusion, these results indicated that Kbz exhibits a broad distribution on the proteome, and the two enzymes regulate various cellular processes through differences in substrate debenzoylation.

SIRT3-regulated K73bz and K197bz of PPIF attenuate their interactions with p53

In general, PTM can exert profound effects on protein expression, activity, and interactions. To explore whether Kbz could impact the MF of proteins, we focused on a benzoylated protein, PPIF, based on the proteomics data, the functional importance of PPIF, and the critical role of the modified site.[16,17] Previous studies have demonstrated that PPIF interacts with the tumor suppressor p53 to trigger necrosis.[18,19] Thus, we hypothesized that the benzoylation of PPIF might interfere with this process. Mass spectrometry data revealed that SIRT3 specifically regulates the benzoylation of PPIF at K73 and K197 (Figure 4A). To validate these findings, we overexpressed FLAG-tagged PPIF in cells and observed a significant increase in PPIF Kbz levels following SB stimulation (Figure 4B). Notably, the Kbz signal of PPIF markedly weakened when lysine residues at positions 73 and 197 were mutated to alanine, indicating that they are the primary Kbz sites on PPIF (Figure 4C). Recently, the genetic code expansion technique has allowed the incorporation of benzoylated lysine into specific sites of relevant proteins, thus bringing a unique advantage to the investigation of the function of Kbz.[20–22] To further investigate whether SIRT3 regulates the benzoylation of PPIF at K73/K197, we first employed the strategy to directly express benzoylated PPIF at K73/K197 in cells, and confirmed their interactions with SIRT3 by co-immunoprecipitation (coIP) assay (Figures 4D and S4A). Moreover, an elevated Kbz level of PPIF was observed after SIRT3 knockdown (Figure 4E), while overexpression of SIRT3 resulted in the opposite result (Figure 4F). In addition, an *in vitro*

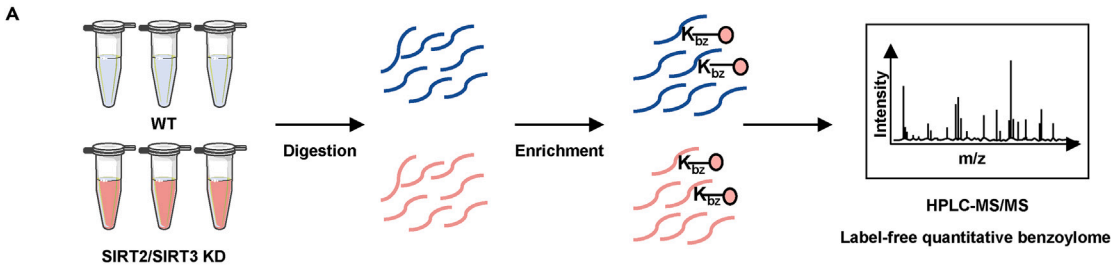
A
WT
SIRT2/SIRT3 KD
Digestion
Enrichment
Intensity
m/z
HPLC-MS/MS
Label-free quantitative benzoylome

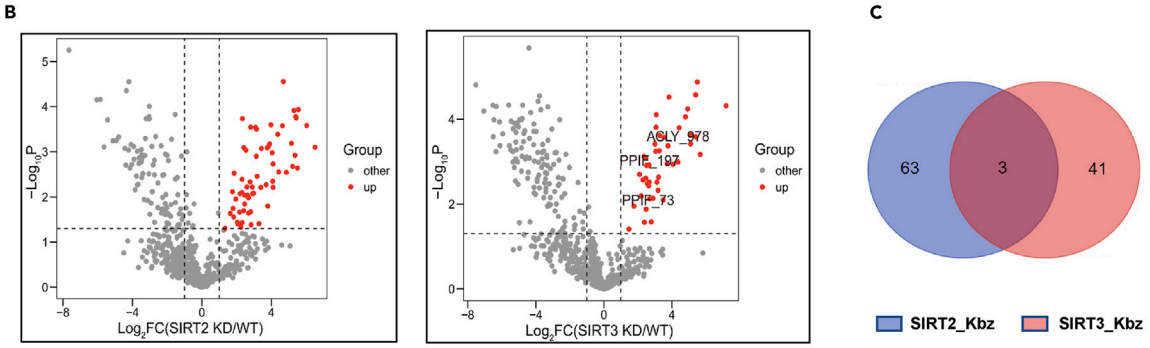
B
Group
other
up
Log2FC(SIRT2 KD/WT)
Log2FC(SIRT3 KD/WT)
ASLY_978
PPIF_197
PPIF_73
C
63
3
41
SIRT2_Kbz
SIRT3_Kbz

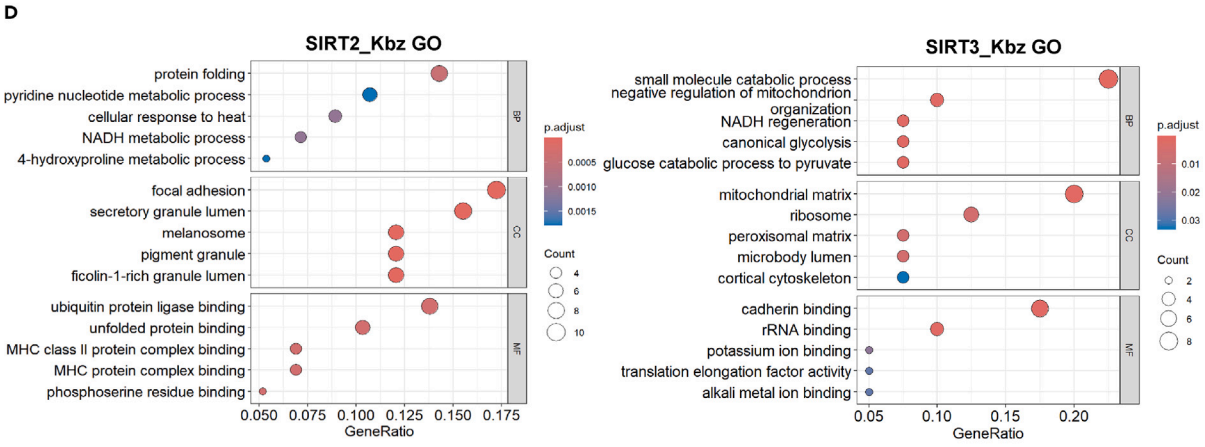
D
SIRT2_Kbz GO
protein folding
pyridine nucleotide metabolic process
cellular response to heat
NADH metabolic process
4-hydroxyproline metabolic process
focal adhesion
secretory granule lumen
melanosome
pigment granule
ficolin-1-rich granule lumen
ubiquitin protein ligase binding
unfolded protein binding
MHC class II protein complex binding
MHC protein complex binding
phosphoserine residue binding
BP
CC
MF
p.adjust
Count
GeneRatio
SIRT3_Kbz GO
small molecule catabolic process
negative regulation of mitochondrion organization
NADH regeneration
canonical glycolysis
glucose catabolic process to pyruvate
mitochondrial matrix
ribosome
peroxisomal matrix
microbody lumen
cortical cytoskeleton
cadherin binding
rRNA binding
potassium ion binding
translation elongation factor activity
alkali metal ion binding

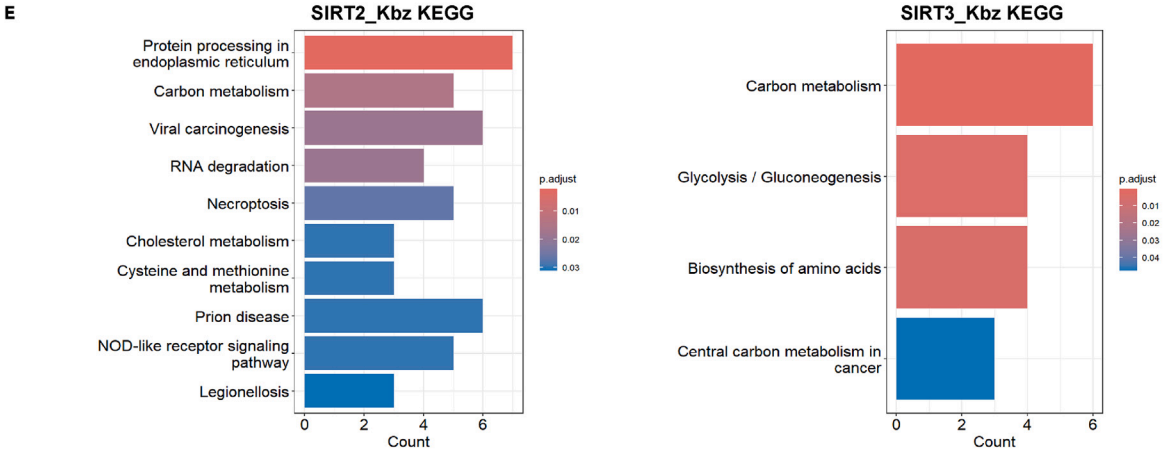
E
SIRT2_Kbz KEGG
Protein processing in endoplasmic reticulum
Carbon metabolism
Viral carcinogenesis
RNA degradation
Necroptosis
Cholesterol metabolism
Cysteine and methionine metabolism
Prion disease
NOD-like receptor signaling pathway
Legionellosis
p.adjust
Count
SIRT3_Kbz KEGG
Carbon metabolism
Glycolysis / Gluconeogenesis
Biosynthesis of amino acids
Central carbon metabolism in cancer

Figure 3. Differential regulation of Kbz sites by SIRT2 and SIRT3

(A) Workflow for the identification of the benzoylome. HepG2 cells treated with 10 mM SB were collected with or without inductive SIRT2 and SIRT3 knockdown. Whole-cell lysates were extracted, trypsin-digested into peptides, and benzoylated peptides were enriched with anti-pan Kbz antibody-conjugated agarose beads, followed by HPLC-MS/MS analysis.

(B) Volcano plots illustrating differential changes in Kbz sites. Red dots represent sites significantly upregulated after knockdown of SIRT2 or SIRT3 (FC > 2, $p < 0.05$).

(C) Venn diagram depicting the number of Kbz sites regulated by SIRT2 and SIRT3.

(D) GO analysis of SIRT2-and SIRT3-mediated Kbz proteins.

(E) KEGG analysis of SIRT2-and SIRT3-regulated Kbz proteins.

debenzoylation assay demonstrated a significant reduction in Kbz levels after incubating PPIF K73bz and K197bz with SIRT3 (Figure S4B). However, inducible knockdown of SIRT2 did not enhance Kbz levels of PPIF K73/K197 (Figure S4C), confirming that SIRT3, but not SIRT2, controls the benzoylation marks on PPIF K73/K197. To elucidate the functional consequences of benzoylated PPIF, we examined how PPIF mutants interacted with p53. The results indicated that PPIF K73/197A mutants significantly attenuated their interactions with p53 (Figure 4G), suggesting that benzoylated PPIF might influence this interaction. Consistent with this, the interaction decreased when PPIF was stimulated by SB (Figure 4H). To directly illustrate the effect of benzoyl-PPIF, we expressed PPIF K73/197bz in cells using the aforementioned method. In line with previous findings, PPIF K73/197bz dramatically reduced the interaction with p53 compared to wild-type (WT) (Figure 4I). In summary, our results demonstrated that SIRT3-regulated PPIF K73/197bz impairs its interaction with the well-known tumor suppressor p53, suggesting a potential influence on specific biological pathways.

SIRT3-regulated ACLY K978bz leads to reduced enzymatic activity

ACLY, a pivotal enzyme linking glucose catabolism to cholesterol and fatty acid synthesis and metabolism,[23] catalyzes the conversion of citric acid into acetyl coenzyme A (CoA) and oxaloacetate in the cytoplasm, requiring ATP and CoA. Benzoylome data showed that SIRT3, but not SIRT2, modulated ACLY K978bz (Figure 5A). To validate the benzoylation of this site by a mass spectrometry-independent method, we expressed FLAG-tagged ACLY in cells and found that the Kbz level significantly increased upon SB stimulation, whereas it clearly decreased when the K978 site was mutated from lysine to alanine (Figures 5B and 5C). To further substantiate the regulatory role of SIRT3 on ACLY K978bz, we introduced FLAG-ACLY K978bz into cells using a non-natural amino acid system and simultaneously overexpressed SIRT3. Our results indicated an interaction between the two, with SIRT3 overexpression leading to a significant reduction in ACLY's Kbz levels at K978 (Figures 5D and S5A). Conversely, inducible knockdown of SIRT3, but not SIRT2, by doxycycline significantly upregulated its Kbz levels (Figures 5E and S5B). Consistent observations were confirmed *in vitro* (Figure 5F). Given the molecular significance of ACLY and this site,[24,25] we explored whether K978bz affected its enzymatic activity. Consequently, we compared ACLY enzyme activity between WT and K978A mutant (Figure S5C), revealing a substantial decrease in the latter (Figure 5G). We postulated that ACLY K978bz would induce a similar perturbation. Indeed, the enzyme activity of both endogenous benzoylated ACLY, stimulated by SB, and exogenously expressed ACLY K978bz, was noticeably lower than that of the WT (Figures 5H and 5I). In conclusion, the results suggest that SIRT3-regulated ACLY K978bz significantly impairs its enzyme activity, thus potentially influencing key metabolic processes.

DISCUSSION

In eukaryotes, certain histone acylations, such as the well-established Kac, neutralize the positive charge on lysine residues, leading to reduced chromatin binding to negatively charged acidic DNA, thereby influencing gene transcription. Histone Kbz has been identified in human, mouse, drosophila, and yeast cells in previous studies.[4,11] Similar to other lysine acylations, histone Kbz possesses distinctive physicochemical properties and is closely linked to the expression of specific genes involved in glycerophospholipid metabolism, ovarian steroidogenesis, and the phospholipase D signaling pathway.[4] Despite recent advancements, further exploration is needed regarding the regulatory elements for this PTM.

In our previous study, we screened the debenzoylase activities of SIRTs and HDACs using a single H2BK5bz peptide and identified the SIRT2 as a debenzoylase. Emerging evidence indicates that SIRT members may exhibit distinct substrate preferences. For instance, SIRT3 failed to remove histone Kbhb if the modified site is flanked by glycine residues.[26] To address this, in this study, we investigated debenzoylase activities of SIRTs using core histones with relatively high Kbz levels as substrates. The results demonstrated that SIRT1 and SIRT3, in addition to the previously reported SIRT2, act as debenzoylases and SIRT3 exhibits stronger activity. Numerous studies have demonstrated that SIRT3 plays crucial roles in various pathophysiological processes, including autophagy,[27] endothelial metabolism,[28] angiogenesis,[28] cardiovascular diseases,[28,29] aging and cancer,[30] and neurodegenerative disorders.[31] Therefore, elucidating the SIRT3-mediated Kbz substrate profile will provide a molecular basis for understanding the potential mechanism of SIRT3 in these physiological processes and diseases through Kbz regulation.

To further comprehend the differential regulation of SIRT3 compared to the previously reported SIRT2 on Kbz, we performed quantitative benzoylome analysis, identifying 44 SIRT3-mediated and 66 SIRT2-mediated Kbz sites, respectively. Interestingly, the SIRT3-and SIRT2-mediated Kbz sites are distinct, with only three being co-regulated by both debenzoylases. Notably, knockdown of SIRT2/3 led to downregulation of some Kbz sites, possibly due to the cellular compensatory mechanisms and signaling network rearrangements. Additionally, SIRT2 and SIRT3 may recognize distinct substrate sequences. Importantly, the two Kbz assemblies are enriched for different biological functions and

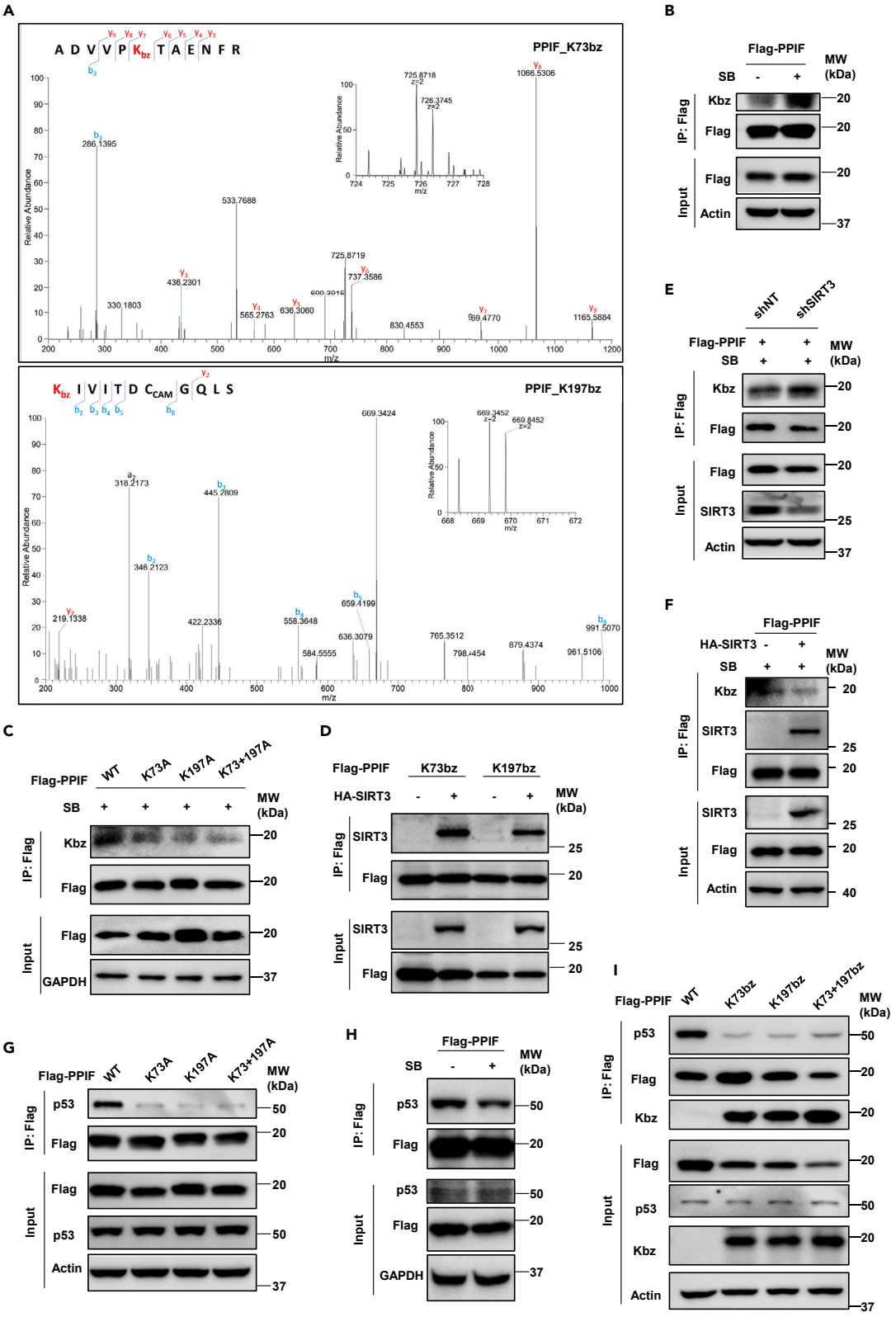
A
PPIF_K73bz
PPIF_K197bz
B
Flag-PPIF
SB
MW (kDa)
IP: Flag
Kbz
Flag
Input
Actin
C
Flag-PPIF
WT
K73A
K197A
K73+197A
GAPDH
D
K73bz
K197bz
HA-SIRT3
SIRT3
E
shNT
shSIRT3
F
G
p53
H
I
K73+197bz

Figure 4. PPIF K73/197bz regulated by SIRT3 attenuates its interaction with p53

(A) MS/MS spectra of PPIF K73bz and K197bz. The b ion refers to the N-terminal parts of the peptide, and the y ion refers to the C-terminal parts of the peptide.

(B) Increased Kbz levels of PPIF in response to SB. FLAG-tagged PPIF was overexpressed in 293T cells with 10 mM SB treatment for 24 h. Whole-cell lysates were collected for IP assay with anti-FLAG antibody-conjugated agarose beads and analyzed by immunoblotting with appropriate antibodies.

(C) Significant attenuation of Kbz levels in PPIF K73/197A mutant. WT and K-A mutant FLAG-PPIF were overexpressed in 293T cells, and whole-cell lysates were collected after 10 mM SB treatment for 24 h for IP assay and immunoblotting analysis.

(D) Interactions between PPIF K73/197bz and SIRT3. FLAG-tagged PPIF K73/197bz and HA-tagged SIRT3 were co-expressed in 293T cells, and the cells were harvested 48 h later for coIP assay and immunoblotting analysis.

(E) Increased Kbz levels of PPIF upon knockdown of SIRT3. FLAG-PPIF was overexpressed in 293T cells stably knockdown of SIRT3 or not, and the cells treated with 10 mM SB for 24 h were harvested for IP assay and immunoblotting analysis.

(F) Reduced Kbz levels of PPIF after SIRT3 overexpression. FLAG-PPIF and HA-vector/SIRT3 were simultaneously expressed in 293T cells, and then the cells treated with 10 mM SB for 24 h were harvested for coIP assay and immunoblot analysis.

(G) Impaired interaction of PPIF K73/197A mutant with p53. Wild-type and K-A mutant FLAG-PPIF were transfected into 293T cells for 48 h, and then whole-cell lysates were extracted for coIP assay and immunoblotting analysis.

(H) Weakened interaction of benzoylated PPIF with p53. FLAG-PPIF was transfected in 293T cells treated with 10 mM SB for 24 h. Whole-cell lysate was collected for coIP assay and subsequent immunoblotting analysis.

(I) Significant reduction in the interaction of PPIF K73/197bz with p53. FLAG-PPIF K73/197bz was overexpressed in 293T cells using genetic codon expansion technology, whole-cell lysates were collected 48 h after transfection for coIP assay and immunoblotting analysis.

cellular pathways, likely attributed to the different subcellular locations of the two erasers. SIRT3 primarily exists in mitochondria,[32,33] mediating substrates closely related to mitochondrial pathways, such as negative regulation of mitochondrion organization, NADH regeneration, and carbon metabolism, with the cytoplasmic component of the substrate predominantly located in the mitochondrial matrix. In contrast, SIRT2 is primarily distributed in the cytoplasm,[33] with its substrate enrichment functions and pathways closely associated with cytosolic and membranous components, including protein folding, ubiquitin protein ligase binding, and protein processing in endoplasmic reticulum. Notably, a subset of Kbz substrates regulated by either SIRT2 or SIRT3 can participate in shared biological processes, such as carbon metabolism pathways, suggesting a vital role for Kbz in metabolism, with potential implications in various pathophysiological processes through metabolic regulation.

Histone Kac is typically linked to gene expression,[34–39] whereas acylation on non-histone proteins is more prevalent and exerts regulatory effects beyond transcription.[14,40–43] For instance, recently discovered Kla is widely distributed throughout the proteome, targeting metabolism-related pathways in hepatocellular carcinoma, with elevated Kla levels of enzymes on these pathways strongly associated with cancer development.[14] Here, we observed that Kbz has a wide distribution on non-histone proteins as well. We experimentally confirmed that PPIF K73/197bz significantly impedes its binding to the tumor suppressor p53, potentially affecting cellular responses, including cell cycle and apoptosis, and may play a role in cancer progression.[18,19,44–46] According to previous studies, this could be due to the fact that K73 is located in the domain where PPIF binds to p53,[16] while K197bz may regulate the amount of binding to p53 by altering its own spatial conformation or translocating between the mitochondrial matrix and the inner membrane. Furthermore, Kbz of another crucial metabolic enzyme, ACLY K978bz, significantly inhibits its own enzymatic activity. Structurally, K978 is spatially very close to the active site of the C-terminal citryl-CoA lyase (CCL) domain (838–1,101 amino acids [aa]) of ACLY, suggesting that small perturbations at this site, such as benzoylation, may affect the enzymatic activity of ACLY.[25] As ACLY is a key enzyme in the cholesterol biosynthesis pathway, reduced activity may impair cholesterol and fatty acid biosynthesis, potentially triggering metabolic diseases.[23,47–49]

Kbz is driven by SB. As a food preservative approved by the US Food and Drug Administration (FDA), the maximum allowable concentration in food is 0.1%, which is generally considered safe, but excessive intake can still cause harm.[50,51] Additionally, SB has been used to treat hyperammonemia,[52] where plasma SB concentrations can rise to approximately 10 mM, a level that may cause severe complications.[53] These findings suggest a close relationship between human health and SB, yet the underlying biological mechanisms remain to be further explored. Current evidence indicates that high levels of histone and non-histone Kbz can be observed in the presence of 5/10 mM SB.[11,54] Further research suggests that benzoylation may influence cellular activities by regulating gene expression,[54] protein-protein interactions such as the K73/K197bz of PPIF, and metabolic enzyme activity such as the K978bz of ACLY in this study, thereby impacting human health. Moreover, benzoylation may serve as an important biomarker for certain diseases, particularly cancers and metabolic disorders. Therefore, a deeper understanding of the regulatory mechanisms of benzoylation could provide clues for the development of new therapeutic approaches.

In conclusion, this study has not only identified crucial regulatory elements in the Kbz pathway beyond SIRT2, but has also systematically and comprehensively characterized the benzoylome differentially regulated by SIRT3 and SIRT2 in mammalian cells. We have preliminarily elucidated the biological functions of Kbz in several important proteins, greatly expanding our understanding of the proteins and functions associated with this newly discovered modification. These results provide valuable insights that may have implications for disease development and therapy.

Limitations of the study

In this study, we discovered that not only SIRT2, but also SIRT1 and SIRT3, can remove Kbz both *in vitro* and in cells. Using mass spectrometry, we identified Kbz-modified proteins and sites specifically regulated by SIRT2 and SIRT3 in mammalian cells. Notably, we demonstrated that

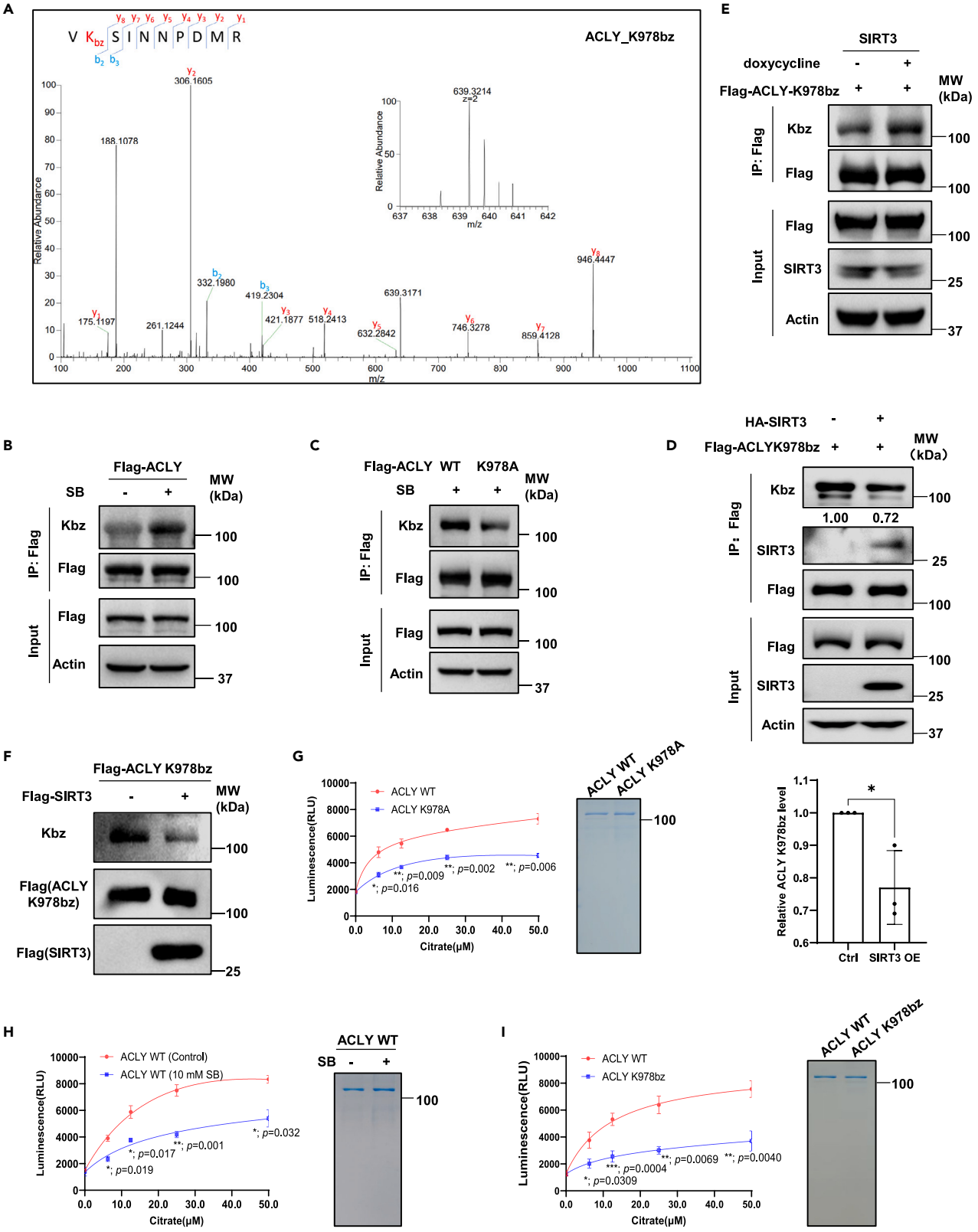
A
V Kbz S I N N P D M R
ACLY_K978bz
Relative Abundance
m/z
306.1605
188.1078
639.3214
z=2
946.4447
639.3171
332.1980
419.2304
421.1877
518.2413
632.2842
746.3278
859.4128
175.1197
261.1244
E
SIRT3
doxycycline - +
Flag-ACLY-K978bz + +
MW (kDa)
IP: Flag
Kbz
Flag
Input
Flag
SIRT3
Actin
100
25
37
B
Flag-ACLY
SB - +
MW (kDa)
IP: Flag
Kbz
Flag
Input
Flag
Actin
C
Flag-ACLY WT K978A
SB + +
MW (kDa)
IP: Flag
Kbz
Flag
Input
Flag
Actin
D
HA-SIRT3 - +
Flag-ACLYK978bz + +
MW (kDa)
IP: Flag
Kbz
1.00 0.72
SIRT3
Flag
Input
Flag
SIRT3
Actin
F
Flag-ACLY K978bz
Flag-SIRT3 - +
MW (kDa)
Kbz
Flag(ACLY K978bz)
Flag(SIRT3)
G
ACLY WT
ACLY K978A
Luminescence(RLU)
Citrate(μM)
*; p=0.016
**; p=0.009
**; p=0.002
**; p=0.006
ACLY WT
ACLY K978A
Relative ACLY K978bz level
Ctrl
SIRT3 OE
H
ACLY WT (Control)
ACLY WT (10 mM SB)
Luminescence(RLU)
Citrate(μM)
*; p=0.019
*; p=0.017
**; p=0.001
*; p=0.032
ACLY WT
SB - +
I
ACLY WT
ACLY K978bz
Luminescence(RLU)
Citrate(μM)
*; p=0.0309
***; p=0.0004
**; p=0.0069
**; p=0.0040
ACLY WT
ACLY K978bz

Figure 5. SIRT3-regulated ACLY K978bz results in reduced enzymatic activity

(A) MS/MS spectra of ACLY K978bz. The b ion refers to the N-terminal parts of the peptide, and the y ion refers to the C-terminal parts of the peptide.

(B) Upregulation of ACLY's Kbz level upon SB stimulation. FLAG-ACLY was transfected in 293T cells, which were then treated with or without 10 mM SB for 24 h and finally harvested for IP and immunoblotting analysis.

(C) Decreased Kbz level when K was mutated to A at 978 of ACLY. Overexpression of wild-type and mutant (K978A) ACLY in 293T cells, the cells were harvested for IP and WB analyses after 24 h of SB treatment.

(D) Significantly decreased Kbz level at 978 of ACLY after SIRT3 overexpression. FLAG-ACLY K978bz and HA-SIRT3 were simultaneously overexpressed in 293T cells. Whole-cell lysates were extracted for coIP assay and immunoblotting analysis 48 h after transfection. Data are represented as mean ± SEM. $n = 3$, biologically independent sample. p value was assessed by one-sided Student's t test. $^{*}p < 0.05$; $^{**}p < 0.01$.

(E) Elevated levels of K978bz in ACLY after SIRT3 inducible knockdown. FLAG-ACLY K978bz was directly expressed in 293T cells, while SIRT3 knockdown was induced by 1 μg/mL doxycycline. Whole-cell lysates were extracted for IP assay and immunoblotting analysis.

(F) SIRT3 removal of K978bz mark from ACLY *in vitro*. FLAG-ACLY K978bz and FLAG-SIRT3 purified from 293T cells were co-incubated *in vitro*, and the Kbz level of ACLY in response to SIRT3 were detected by immunoblotting.

(G) Weakened enzyme activity of ACLY K978A mutant. Enzyme activity assay was determined using ADP-Glo Kinase Assay Kit. Data are represented as mean ± SEM. $n = 3$, biologically independent sample. p value was assessed by one-sided Student's t test. $^{*}p < 0.05$; $^{**}p < 0.01$.

(H) Impaired enzyme activity of benzoylated ACLY by SB. Enzyme activity assay was determined using ADP-Glo Kinase Assay Kit. Data are represented as mean ± SEM. $n = 3$, biologically independent sample. p value was assessed by two-sided Student's t test. $^{*}p < 0.05$; $^{**}p < 0.01$.

(I) Attenuated enzyme activity of the ACLY K978bz. Enzyme activity assay was determined using ADP-Glo Kinase Assay Kit. Data are represented as mean ± SEM. $n = 3$, biologically independent sample. p value was assessed by two-sided Student's t test. $^{*}p < 0.05$; $^{**}p < 0.01$; $^{***}p < 0.001$.

Kbz can influence the interaction between PPIF and p53, as well as the enzymatic activity of ACLY. However, whether Kbz modifications contribute to disease progression by altering the function of these proteins requires further investigation.

RESOURCE AVAILABILITY

Lead contact

Further information and requests for resources and reagents should be directed to the lead contact, He Huang (hhuang@simm.ac.cn).

Materials availability

All materials and unique reagents described in this study are available from the lead contact upon reasonable request.

Data and code availability

- The mass spectrometry proteomics data have been deposited to the ProteomeXchange Consortium via the PRIDE partner repository with the dataset identifier PXD047031.
- This paper does not report original code.
- Any additional information required to reanalyze the data reported in this paper is available from the lead contact upon request.

ACKNOWLEDGMENTS

This research is supported by the National Natural Science Foundation of China (22277125 and 92253306 to H.H.), Natural Science Foundation of Shanghai (23ZR1474600 to H.H.), and the Shanghai Municipal Science and Technology Major Project (to H.H.).

AUTHOR CONTRIBUTIONS

H.H. conceived the research and designed the studies. P.P. performed most of the biological experiments, and wrote the manuscript. Y.L., C.Y., and X.G. were involved in the biological experiments. X.R. and X.S. performed the mass spectrometry analysis and data analysis. R.L. provided advice for the biological experiments. H.H. supervised the study and revised the manuscript. All authors have approved the final version.

DECLARATION OF INTERESTS

The authors declare no competing interests.

STAR★METHODS

Detailed methods are provided in the online version of this paper and include the following:

- *In vitro* debenzoylation assay
- ATP-citrate lyase enzyme activity assay
- Protein extraction for proteomics
- Trypsin digestion
- Pan Kbz-based post-translational modification enrichment
- HPLC-MS/MS analysis of Kbz
- Protein sequence database searching
- Bioinformatics analysis

- QUANTIFICATION AND STATISTICAL ANALYSIS

SUPPLEMENTAL INFORMATION

Supplemental information can be found online at https://doi.org/10.1016/j.isci.2024.111176.

Received: February 29, 2024
Revised: August 26, 2024
Accepted: October 11, 2024
Published: October 16, 2024

REFERENCES

1. Sabari, B.R., Tang, Z., Huang, H., Yong-Gonzalez, V., Molina, H., Kong, H.E., Dai, L., Shimada, M., Cross, J.R., Zhao, Y., et al. (2015). Intracellular crotonyl-CoA stimulates transcription through p300-catalyzed histone crotonylation. Mol. Cell *58*, 203–215. https://doi.org/10.1016/j.molcel.2015.02.029.
2. Xie, Z., Zhang, D., Chung, D., Tang, Z., Huang, H., Dai, L., Qi, S., Li, J., Colak, G., Chen, Y., et al. (2016). Metabolic Regulation of Gene Expression by Histone Lysine beta-Hydroxybutyrylation. Mol. Cell *62*, 194–206. https://doi.org/10.1016/j.molcel.2016.03.036.
3. Zhao, D., Li, Y., Xiong, X., Chen, Z., and Li, H. (2017). YEATS Domain-A Histone Acylation Reader in Health and Disease. J. Mol. Biol. *429*, 1994–2002. https://doi.org/10.1016/j.jmb.2017.03.010.
4. Huang, H., Zhang, D., Wang, Y., Perez-Neut, M., Han, Z., Zheng, Y.G., Hao, Q., and Zhao, Y. (2018). Lysine benzoylation is a histone mark regulated by SIRT2. Nat. Commun. *9*, 3374. https://doi.org/10.1038/s41467-018-05567-w.
5. Zhang, D., Tang, Z., Huang, H., Zhou, G., Cui, C., Weng, Y., Liu, W., Kim, S., Lee, S., Perez-Neut, M., et al. (2019). Metabolic regulation of gene expression by histone lactylation. Nature *574*, 575–580. https://doi.org/10.1038/s41586-019-1678-1.
6. Yi, X., Jiang, X., Li, X., and Jiang, D.S. (2017). Histone lysine methylation and congenital heart disease: From bench to bedside (Review). Int. J. Mol. Med. *40*, 953–964. https://doi.org/10.3892/ijmm.2017.3115.
7. Wesseling, H., Mair, W., Kumar, M., Schlaffner, C.N., Tang, S., Beerepoot, P., Fatou, B., Guise, A.J., Cheng, L., Takeda, S., et al. (2020). Tau PTM Profiles Identify Patient Heterogeneity and Stages of Alzheimer's Disease. Cell *183*, 1699–1713.e13. https://doi.org/10.1016/j.cell.2020.10.029.
8. Jiang, Y., Li, Y., Liu, C., Zhang, L., Lv, D., Weng, Y., Cheng, Z., Chen, X., Zhan, J., and Zhang, H. (2021). Isonicotinylation is a histone mark induced by the anti-tuberculosis first-line drug isoniazid. Nat. Commun. *12*, 5548. https://doi.org/10.1038/s41467-021-25867-y.
9. Seto, E., and Yoshida, M. (2014). Erasers of histone acetylation: the histone deacetylase enzymes. Cold Spring Harb. Perspect. Biol. *6*, a018713. https://doi.org/10.1101/cshperspect.a018713.
10. Vaquero, A., Sternglanz, R., and Reinberg, D. (2007). NAD+-dependent deacetylation of H4 lysine 16 by class III HDACs. Oncogene *26*, 5505–5520. https://doi.org/10.1038/sj.onc.1210617.
11. Wang, D., Yan, F., Wu, P., Ge, K., Li, M., Li, T., Gao, Y., Peng, C., and Chen, Y. (2022). Global profiling of regulatory elements in the histone benzoylation pathway. Nat. Commun. *13*, 1369. https://doi.org/10.1038/s41467-022-29057-2.
12. Huang, H., Luo, Z., Qi, S., Huang, J., Xu, P., Wang, X., Gao, L., Li, F., Wang, J., Zhao, W., et al. (2017). Landscape of the regulatory elements for lysine 2-hydroxyisobutyrylation pathway. Cell Res. *28*, 111–125. https://doi.org/10.1038/cr.2017.149.
13. Tan, D., Wei, W., Han, Z., Ren, X., Yan, C., Qi, S., Song, X., Zheng, Y.G., Wong, J., and Huang, H. (2022). HBO1 catalyzes lysine benzoylation in mammalian cells. iScience *25*, 105443. https://doi.org/10.1016/j.isci.2022.105443.
14. Yang, Z., Yan, C., Ma, J., Peng, P., Ren, X., Cai, S., Shen, X., Wu, Y., Zhang, S., Wang, X., et al. (2023). Lactylome analysis suggests lactylation-dependent mechanisms of metabolic adaptation in hepatocellular carcinoma. Nat. Metab. *5*, 61–79. https://doi.org/10.1038/s42255-022-00710-w.
15. Huang, H., Zhang, D., Weng, Y., Delaney, K., Tang, Z., Yan, C., Qi, S., Peng, C., Cole, P.A., Roeder, R.G., and Zhao, Y. (2021). The regulatory enzymes and protein substrates for the lysine β-hydroxybutyrylation pathway. Sci. Adv. *7*, eabe2771. https://doi.org/10.1126/sciadv.abe2771.
16. Fayaz, S.M., and Rajanikant, G.K. (2015). Modelling the molecular mechanism of protein–protein interactions and their inhibition: CypD–p53 case study. Mol. Divers. *19*, 931–943. https://doi.org/10.1007/s11030-015-9612-4.
17. Davis, T.L., Walker, J.R., Campagna-Slater, V., Finerty, P.J., Paramanathan, R., Bernstein, G., MacKenzie, F., Tempel, W., Ouyang, H., Lee, W.H., et al. (2010). Structural and Biochemical Characterization of the Human Cyclophilin Family of Peptidyl-Prolyl Isomerases. PLoS Biol. *8*, e1000439. https://doi.org/10.1371/journal.pbio.1000439.
18. Zavileyskiy, L., and Bunik, V. (2022). Regulation of p53 Function by Formation of Non-Nuclear Heterologous Protein Complexes. Biomolecules *12*, 327. https://doi.org/10.3390/biom12020327.
19. Vaseva, A.V., Marchenko, N.D., Ji, K., Tsirka, S.E., Holzmann, S., and Moll, U.M. (2012). p53 opens the mitochondrial permeability transition pore to trigger necrosis. Cell *149*, 1536–1548. https://doi.org/10.1016/j.cell.2012.05.014.
20. Cao, L., Liu, J., Ghelichkhani, F., Rozovsky, S., and Wang, L. (2021). Genetic Incorporation of ϵ-N-Benzoyllysine by Engineering Methanomethylophilus alvus Pyrrolysyl-tRNA Synthetase. Chembiochem *22*, 2530–2534. https://doi.org/10.1002/cbic.202100218.
21. Ji, Y., Ren, C., Miao, H., Pang, Z., Xiao, R., Yang, X., and Xuan, W. (2021). Genetically encoding ε-N-benzoyllysine in proteins. Chem. Commun. *57*, 1798–1801. https://doi.org/10.1039/d0cc07954e.
22. Tian, H., Yang, J., Guo, A.-D., Ran, Y., Yang, Y.-Z., Yang, B., Huang, R., Liu, H., and Chen, X.-H. (2021). Genetically Encoded Benzoyllysines Serve as Versatile Probes for Interrogating Histone Benzoylation and Interactions in Living Cells. ACS Chem. Biol. *16*, 2560–2569. https://doi.org/10.1021/acschembio.1c00614.
23. Feng, X., Zhang, L., Xu, S., and Shen, A.Z. (2020). ATP-citrate lyase (ACLY) in lipid metabolism and atherosclerosis: An updated review. Prog. Lipid Res. *77*, 101006. https://doi.org/10.1016/j.plipres.2019.101006.
24. Irina, A., Potapova, M.R.E.-M., Doronin, S.V., and Benjamin, W.B. (2000). Phosphorylation of Recombinant Human ATP:Citrate Lyase by cAMP-Dependent Protein Kinase Abolishes Homotropic Allosteric Regulation of the Enzyme by Citrate and Increases the Enzyme Activity. Allosteric Activation of ATP:Citrate Lyase by Phosphorylated Sugars. Biochemistry *39*, 1169–1179. https://doi.org/10.1021/bi992159y.
25. Verschueren, K.H.G., Blanchet, C., Felix, J., Dansercoer, A., De Vos, D., Bloch, Y., Van Beeumen, J., Svergun, D., Gutsche, I., Savvides, S.N., and Verstraete, K. (2019). Structure of ATP citrate lyase and the origin of citrate synthase in the Krebs cycle. Nature *568*, 571–575. https://doi.org/10.1038/s41586-019-1095-5.
26. Zhang, X., Cao, R., Niu, J., Yang, S., Ma, H., Zhao, S., and Li, H. (2019). Molecular basis for

hierarchical histone de-beta-hydroxybutyrylation by SIRT3. Cell Discov. *5*, 35. https://doi.org/10.1038/s41421-019-0103-0.

27. Zheng, Y., Shi, B., Ma, M., Wu, X., and Lin, X. (2019). The novel relationship between Sirt3 and autophagy in myocardial ischemia-reperfusion. J. Cell. Physiol. *234*, 5488–5495. https://doi.org/10.1002/jcp.27329.
28. He, X., Zeng, H., and Chen, J.X. (2019). Emerging role of SIRT3 in endothelial metabolism, angiogenesis, and cardiovascular disease. J. Cell. Physiol. *234*, 2252–2265. https://doi.org/10.1002/jcp.27200.
29. Sun, W., Liu, C., Chen, Q., Liu, N., Yan, Y., and Liu, B. (2018). SIRT3: A New Regulator of Cardiovascular Diseases. Oxid. Med. Cell. Longev. *2018*, 7293861. https://doi.org/10.1155/2018/7293861.
30. Chen, J., Wang, A., and Chen, Q. (2017). SirT3 and p53 Deacetylation in Aging and Cancer. J. Cell. Physiol. *232*, 2308–2311. https://doi.org/10.1002/jcp.25669.
31. Anamika, Khanna, A., Khanna, A., Acharjee, P., Acharjee, A., and Trigun, S.K. (2019). Mitochondrial SIRT3 and neurodegenerative brain disorders. J. Chem. Neuroanat. *95*, 43–53. https://doi.org/10.1016/j.jchemneu.2017.11.009.
32. Schwer, B., North, B.J., Frye, R.A., Ott, M., and Verdin, E. (2002). The human silent information regulator (Sir)2 homologue hSIRT3 is a mitochondrial nicotinamide adenine dinucleotide-dependent deacetylase. J. Cell Biol. *158*, 647–657. https://doi.org/10.1083/jcb.200205057.
33. Michishita, E., Park, J.Y., Burneskis, J.M., Barrett, J.C., and Horikawa, I. (2005). Evolutionarily conserved and nonconserved cellular localizations and functions of human SIRT proteins. Mol. Biol. Cell *16*, 4623–4635. https://doi.org/10.1091/mbc.e05-01-0033.
34. Sabari, B.R., Zhang, D., Allis, C.D., and Zhao, Y. (2017). Metabolic regulation of gene expression through histone acylations. Nat. Rev. Mol. Cell Biol. *18*, 90–101. https://doi.org/10.1038/nrm.2016.140.
35. Barnes, C.E., English, D.M., and Cowley, S.M. (2019). Acetylation & Co: an expanding repertoire of histone acylations regulates chromatin and transcription. Essays Biochem. *63*, 97–107. https://doi.org/10.1042/EBC20180061.
36. Li, K., and Wang, Z. (2021). Histone crotonylation-centric gene regulation. Epigenet. Chromatin *14*, 10. https://doi.org/10.1186/s13072-021-00385-9.
37. Liu, J., Shangguan, Y., Tang, D., and Dai, Y. (2021). Histone succinylation and its function on the nucleosome. J. Cell Mol. Med. *25*, 7101–7109. https://doi.org/10.1111/jcmm.16676.
38. Gao, Y., Sheng, X., Tan, D., Kim, S., Choi, S., Paudel, S., Lee, T., Yan, C., Tan, M., Kim, K.M., et al. (2023). Identification of Histone Lysine Acetoacetylation as a Dynamic Post-Translational Modification Regulated by HBO1. Adv. Sci. *10*, e2300032. https://doi.org/10.1002/advs.202300032.
39. Tan, M., Luo, H., Lee, S., Jin, F., Yang, J.S., Montellier, E., Buchou, T., Cheng, Z., Rousseaux, S., Rajagopal, N., et al. (2011). Identification of 67 histone marks and histone lysine crotonylation as a new type of histone modification. Cell *146*, 1016–1028. https://doi.org/10.1016/j.cell.2011.08.008.
40. Shvedunova, M., and Akhtar, A. (2022). Modulation of cellular processes by histone and non-histone protein acetylation. Nat. Rev. Mol. Cell Biol. *23*, 329–349. https://doi.org/10.1038/s41580-021-00441-y.
41. Tong, Y., Guo, D., Lin, S.H., Liang, J., Yang, D., Ma, C., Shao, F., Li, M., Yu, Q., Jiang, Y., et al. (2021). SUCLA2-coupled regulation of GLS succinylation and activity counteracts oxidative stress in tumor cells. Mol. Cell *81*, 2303–2316.e8. https://doi.org/10.1016/j.molcel.2021.04.002.
42. Koronowski, K.B., Greco, C.M., Huang, H., Kim, J.K., Fribourgh, J.L., Crosby, P., Mathur, L., Ren, X., Partch, C.L., Jang, C., et al. (2021). Ketogenesis impact on liver metabolism revealed by proteomics of lysine beta-hydroxybutyrylation. Cell Rep. *36*, 109487. https://doi.org/10.1016/j.celrep.2021.109487.
43. Liao, L., He, Y., Li, S.J., Yu, X.M., Liu, Z.C., Liang, Y.Y., Yang, H., Yang, J., Zhang, G.G., Deng, C.M., et al. (2023). Lysine 2-hydroxyisobutyrylation of NAT10 promotes cancer metastasis in an ac4C-dependent manner. Cell Res. *33*, 355–371. https://doi.org/10.1038/s41422-023-00793-4.
44. Bigi, A., Beltrami, E., Trinei, M., Stendardo, M., Pelicci, P.G., and Giorgio, M. (2016). Cyclophilin D counteracts P53-mediated growth arrest and promotes Ras tumorigenesis. Oncogene *35*, 5132–5143. https://doi.org/10.1038/onc.2016.42.
45. Zhen, Y.F., Wang, G.D., Zhu, L.Q., Tan, S.P., Zhang, F.Y., Zhou, X.Z., and Wang, X.D. (2014). P53 dependent mitochondrial permeability transition pore opening is required for dexamethasone-induced death of osteoblasts. J. Cell. Physiol. *229*, 1475–1483. https://doi.org/10.1002/jcp.24589.
46. Lu, J.H., Shi, Z.F., and Xu, H. (2014). The mitochondrial cyclophilin D/p53 complexation mediates doxorubicin-induced non-apoptotic death of A549 lung cancer cells. Mol. Cell. Biochem. *389*, 17–24. https://doi.org/10.1007/s11010-013-1922-1.
47. Ference, B.A., Ray, K.K., Catapano, A.L., Ference, T.B., Burgess, S., Neff, D.R., Oliver-Williams, C., Wood, A.M., Butterworth, A.S., Di Angelantonio, E., et al. (2019). Mendelian Randomization Study of ACLY and Cardiovascular Disease. N. Engl. J. Med. *380*, 1033–1042. https://doi.org/10.1056/NEJMoa1806747.
48. Guo, Q., Kang, H., Wang, J., Dong, Y., Peng, R., Zhao, H., Wu, W., Guan, H., and Li, F. (2021). Inhibition of ACLY Leads to Suppression of Osteoclast Differentiation and Function Via Regulation of Histone Acetylation. J. Bone Miner. Res. *36*, 2065–2080. https://doi.org/10.1002/jbmr.4399.
49. Mohammadi-Shemirani, P., Chong, M., Perrot, N., Pigeyre, M., Steinberg, G.R., Paré, G., Krepinsky, J.C., and Lanktree, M.B. (2022). ACLY and CKD: A Mendelian Randomization Analysis. Kidney Int. Rep. *7*, 1673–1681. https://doi.org/10.1016/j.ekir.2022.04.013.
50. Yılmaz, S., Ünal, F., and Yüzbaşıoğlu, D. (2009). The in vitro genotoxicity of benzoic acid in human peripheral blood lymphocytes. Cytotechnology *60*, 55–61. https://doi.org/10.1007/s10616-009-9214-z.
51. Pongsavee, M. (2015). Effect of Sodium Benzoate Preservative on Micronucleus Induction, Chromosome Break, and Ala40Thr Superoxide Dismutase Gene Mutation in Lymphocytes. BioMed Res. Int. *2015*, 103512. https://doi.org/10.1155/2015/103512.
52. Brusilow, S.W., Danney, M., Waber, L.J., Batshaw, M., Burton, B., Levitsky, L., Roth, K., McKeethren, C., and Ward, J. (1984). Treatment of episodic hyperammonemia in children with inborn errors of urea synthesis. N. Engl. J. Med. *310*, 1630–1634. https://doi.org/10.1056/NEJM198406213102503.
53. Praphanproj, V., Boyadjiev, S.A., Waber, L.J., Brusilow, S.W., and Geraghty, M.T. (2000). Three cases of intravenous sodium benzoate and sodium phenylacetate toxicity occurring in the treatment of acute hyperammonaemia. J. Inherit. Metab. Dis. *23*, 129–136. https://doi.org/10.1023/a:1005661631281.
54. Huang, H., Zhang, D., Wang, Y., Perez-Neut, M., Han, Z., Zheng, Y.G., Hao, Q., and Zhao, Y. (2018). Lysine benzoylation is a histone mark regulated by SIRT2. Nat. Commun. *9*, 3374. https://doi.org/10.1038/s41467-018-05567-w.
55. Lang, K., and Chin, J.W. (2014). Cellular Incorporation of Unnatural Amino Acids and Bioorthogonal Labeling of Proteins. Chem. Rev. *114*, 4764–4806. https://doi.org/10.1021/cr400355w.
56. Xiao, H., and Schultz, P.G. (2016). At the Interface of Chemical and Biological Synthesis: An Expanded Genetic Code. Cold Spring Harb. Perspect. Biol. *8*, a023945. https://doi.org/10.1101/cshperspect.a023945.
57. Wang, L. (2017). Engineering the Genetic Code in Cells and Animals: Biological Considerations and Impacts. Acc. Chem. Res. *50*, 2767–2775. https://doi.org/10.1021/acs.accounts.7b00376.
58. Shechter, D., Dormann, H.L., Allis, C.D., and Hake, S.B. (2007). Extraction, purification and analysis of histones. Nat. Protoc. *2*, 1445–1457. https://doi.org/10.1038/nprot.2007.202.
59. Yu, G., Wang, L.G., Han, Y., and He, Q.Y. (2012). clusterProfiler: an R package for comparing biological themes among gene clusters. OMICS A J. Integr. Biol. *16*, 284–287. https://doi.org/10.1089/omi.2011.0118.
60. Colaert, N., Helsens, K., Martens, L., Vandekerckhove, J., and Gevaert, K. (2009). Improved visualization of protein consensus sequences by iceLogo. Nat. Methods *6*, 786–787. https://doi.org/10.1038/nmeth1109-786.

STAR★METHODS

KEY RESOURCES TABLE

REAGENT or RESOURCE	SOURCE	IDENTIFIER
Antibodies		
pan Kbz	PTM Biolabs	PTM-761/762
pan Kac	PTM Biolabs	PTM-101/105RM; RRID: AB_2940830/ RRID: AB_3099509
p53	PTM Biolabs	PTM-6319
SIRT1	PTM Biolabs	PTM-MM011
histone H3	Huabio	M1306-4; RRID: AB_3073062
β-actin	Proteintech Group	66009-1-Ig; RRID: AB_2687938
GAPDH	Proteintech Group	60004-1-Ig; RRID: AB_2107436
HA	Proteintech Group	51064-2-AP; RRID: AB_11042321
SIRT2	Proteintech Group	19655-1-AP; RRID: AB_2878592
SIRT3	Proteintech Group	10099-1-AP; RRID: AB_2239240
FLAG	Proteintech Group	20543-1-AP; RRID: AB_11232216
FLAG	Sigma-Aldrich	F1804; RRID: AB_262044
Bacterial and virus strains		
Trans1-T1	TransGen Biotech	CD501-02
BL21	TransGen Biotech	CD701-02
Lentiviral_shSIRT1	This paper	N/A
Lentiviral_shSIRT2	This paper	N/A
Lentiviral_shSIRT3	This paper	N/A
Chemicals, peptides, and recombinant proteins		
sodium butyrate (NaBu)	Sinopharmgroup	XW15654701
nicotinamide (NAM)	Sigma-Aldrich	N3376-100G
Puromycin	Selleck	S7417
doxycycline	TCI	D4116
protease inhibitor cocktail	Bimake	B14011
DMEM medium	Basalmedia	L110KJ
fetal bovine serum (FBS)	Ausbian	WS500T
penicillin/streptomycin	Gibco	15140122
Liposomal Transfection Reagent	Yeasen	40802ES03
sodium benzoate	Sangon Biotech	A600833
benzoylated lysine	This paper	N/A
GSTSep Glutathione Agarose Resin	Yeasen	20507ES50
HisSep Ni-NTA Agarose Resin 6FF	Yeasen	20503ES50
anti-FLAG antibody-conjugated agarose beads	Sigma-Aldrich	A2220-5ML
Critical commercial assays		
ADP-Glo™ Kinase Assay Kit	Promega	V6930
Deposited data		
Proteome and benzoylome data	PRIDE	PXD047031
Experimental models: Cell lines		
293T	National Collection of Authenticated Cell Cultures, China	SCSP-502
HepG2	National Collection of Authenticated Cell Cultures, China	SCSP-510

(*Continued on next page*)

Continued

REAGENT or RESOURCE	SOURCE	IDENTIFIER
Oligonucleotides		
shRNA targeting SIRT1 sequence: 5′-cagctaagagtaatgatga-3′	This paper	N/A
shRNA targeting SIRT2 sequence: 5′-gacttcctgcggaacttat-3′	This paper	N/A
shRNA targeting SIRT3 sequence: 5′-caagtgttgttggaagtgg-3′	This paper	N/A
Recombinant DNA		
FLAG-SIRT1/2/3	This paper	N/A
HA-SIRT1/2/3	This paper	N/A
GST-SIRT1/3/4 (truncated)	This paper	N/A
His-SIRT2 (truncated)/5/6/7 (full-length)	This paper	N/A
pGIPZ-shSIRT1/2/3	This paper	N/A
pTRIPZ-shSIRT1/2/3	This paper	N/A
pNEU-hMbPylRS-4xU6M15 plasmid (modified)	Addgene	addgene#105830
Software and algorithms		
MaxQuant software	Max Planck Institute of Biochemistry	https://www.maxquant.org/
R	R Core Team	https://cran.r-project.org/mirrors.html
GraphPad Prism 9	GraphPad software Inc	https://www.graphpad.com/scientific-software/prism/

EXPERIMENTAL MODEL AND STUDY PARTICIPANT DETAILS

Cell lines

293T and HepG2 cells (National Collection of Authenticated Cell Cultures, China) were cultured in DMEM medium (L110KJ, Basalmedia) supplemented with 10% fetal bovine serum (FBS, WS500T, Ausbian) and 1% penicillin/streptomycin (15140122, Gibco) at 37°C, 5% CO_2. Cells were identified by STR and routinely tested negative for Mycoplasma by PCR.

METHOD DETAILS

Transfection

Transfection was performed following the Hieff Trans Liposomal Transfection Reagent instructions (40802ES03, Yeasen). Briefly, plasmids were transfected into 293T or HepG2 cells for 48 h, with 5/10 mM SB treatment for the last 24 h.

Construction of stable transgenic cell lines

ShRNA was cloned into pGIPZ or pTRIPZ vectors (SIRT1: 5′-cagctaagagtaatgatga-3′; SIRT2: 5′-gacttcctgcggaacttat-3′; SIRT3: 5′-caagtgttgttg gaagtgg-3′), while sgRNA was cloned into the lentiCRISPRv2 vector (SIRT1: 5′-gttgactgtgaagctgtacg-3′; SIRT2: 5′-gcggaacttattctcccaga-3′; SIRT3: 5′-gtacgatctcccgtaccccg-3′). These plasmids were co-transfected with pMD2.G, psPAX2 to form a triple plasmid system for lentiviral packaging into 293T cells. Lentiviral supernatants were collected at 48 h and 72 h post-transfection, then filtered with a 0.22 μm filter membrane (virus concentration depending on the situation). Lentivirus was used to infect 293T or HepG2 cells, and after 2–3 days, cells were treated with 3 μg/mL puromycin (S7417, Selleck) for 3 days to select for stable knockdown or knockout of target genes. For inducible knockdown systems, induction with 1 μg/mL doxycycline (D4116, TCI) for 72 h is required to achieve target gene knockdown.

Western blotting

Harvested 293T or HepG2 cells were washed twice with cold PBS and lysed by ultrasonication, adding 1% SDS lysis buffer containing protease inhibitor cocktail (B14011, Bimake). The protein supernatant was obtained by centrifuging, and protein concentration was determined using a BCA kit (P0010, Beyotime Biotechnology). Using 12% or 15% SDS-PAGE, proteins were separated by electrophoresis. Afterward, proteins on the gel were transferred to a PVDF membrane, which was then blocked in 3% BSA or 5% Blotting Grade Blocker Nonfat Dry Milk for 1 h at room temperature. Membranes were incubated with the specific primary antibody solution overnight at 4°C. Next, the membranes were incubated with the matching secondary antibody solution at room temperature for 1 h after being rinsed three times with TBST. Finally, chemiluminescent detection was performed using ECL luminous solution with a Tanon 4600 (Tanon).

Immunoprecipitation/Co-Immunoprecipitation (IP/Co-Immunoprecipitation)

Cells were harvested after 48 h transfection, washed twice with cold PBS, and lysed in 300 μL of lysis buffer (20 mM Tris pH7.5, 150 mM NaCl, 1% Triton X-100, supplemented with the protease inhibitor cocktail) per well of a six-well plate on ice for 1 h. Whole cell lysate was collected, sonicated (this step was skipped in coIP assay), and centrifuged. A partial supernatant was retained as input, and the remaining was incubated with 5 μL of anti-FLAG antibody-conjugated agarose beads (Sigma-Aldrich, A2220-5ML) at 4°C under rotation for 2 h. After the precipitate was washed three times with lysis buffer/PBS, 1*x* protein loading buffer was added for western blot analysis. Alternatively, 1*x* FLAG peptide (GL Biochem, final concentration of 50 μg/mL) was added to the precipitate after three washes to competitively elute FLAG-tagged proteins used for subsequent analysis.

Genetic code expansion technique

Genetic codon expansion technique refers to the specific recognition of unnatural amino acids and their incorporation into specific sites of proteins by modifying the cellular translational system, in particular tRNAs and the corresponding aminoacyl-tRNA synthetases (aaRS) *in vitro* and in living cells.[55–57] Take eukaryotic expression of FLAG-tagged PPIF K73bz as an example. First, based on previous reports, we mutated MbPylRS (including A271Y&Y349F) on the purchased pNEU-hMbPylRS-4xU6M15 plasmid (Addgene#105830, containing humanized MbPylRS and tRNAM15) to specifically recognize and catalyze the binding of Kbz to the tRNA to form the aminoacyl -tRNA molecule.[20–22] Then, we constructed a eukaryotically expressed C-terminally FLAG-tagged PPIF plasmid and mutated the codon encoding lysine at 73 to amber-mutated termination codon (TAG). Finally, we simultaneously co-transfected the modified pNEU-hMbPylRS-4xU6M15 and 3′-FLAG-PPIF K73TAG into 293T cells and treated them with 1 mM benzoylated lysine (laboratory synthesis) for 48 h before harvesting the cells for subsequent analysis. Since the FLAG tag is located at the C-terminus, if Kbz is not correctly incorporated at positions 73/197 of PPIF, the FLAG signal would not be detected by immunoblotting.

Recombinant protein expression and purification

Truncated SIRT1, SIRT3 and SIRT4 were cloned into the pGEX-4T-1 (GST tag) vector, while truncated SIRT2 and full-length SIRT5-7 were cloned into the PET-28a vector (His tag). These plasmids were transformed into BL21 cells grown overnight at 37°C on LB plates (containing 50 μg/mL ampicillin or 30 μg/mL kanamycin). Monoclonal colonies were selected and incubated overnight in LB medium at 37°C, 220 rpm. The bacteria were injected into a fresh LB medium and incubated until an OD_{600} reached 0.6. IPTG (final concentration 0.1 mM) was administered to active gene expression for at least 2 h at 37°C or overnight at 16°C. The bacteria were gathered by centrifugation and then resuspended in lysis buffer (GST lysis buffer: 1 mM EDTA, 150 mM NaCl, 5% glycerol, 0.2 mM PMSF; His lysis buffer: 50 mM NaH_2PO_4, 300 mM NaCl, 10 mM imidazole pH 8.0, 0.2 mM PMSF) followed by ultrasonic disruption. After centrifugation, the supernatant was transferred to a clean tube. Fill the chromatography column with GST beads (or Ni-NTA beads) and equilibrate them with lysis buffer. Mix the supernatant in the column for 2–4 h at 4°C. Wash the beads 4 times with wash buffer (GST wash buffer: 0.1% Triton X-100; His wash buffer: 50 mM NaH_2PO_4, 300 mM NaCl, 20 mM imidazole pH 8.0, 0.2 mM PMSF), mixing for 5 min at 4°C each time to eliminate contaminants. Next, elute the proteins of interest 5–10 times with elution buffer (GST elution buffer: 50 mM Tris HCl pH 8.0, 10 mM reduced glutathione; His elution buffer: 50 mM NaH_2PO_4, 300 mM NaCl, 250 mM imidazole pH 8.0) and incubate on ice for 5 min each time. The proteins are mixed with 50% glycerol in an equal volume for long-term storage at −80°C.

In vitro SIRTs screening

Histones extracted following a standard acid-extraction protocol[58] were used as the substrates. The reactions were performed in a final volume of 30 μL per well in PCR tubes. For each reaction, 4 μg of histones and 0.5–1 μg of SIRTs were added to the reaction buffer (20 mM Tris pH 8.0, 1 mM DTT, 1 mM NAD^+). After incubation at 37°C for 30 min, the reactions were quenched by heating at 95°C for 5 min. The supernatant was collected by centrifugation and used for immunoblotting analysis.

In vitro debenzoylation assay

Briefly, 0.5 μM Kbz peptide and 0.25 μM SIRT1/2/3 enzyme were added to the reaction buffer (20 mM Tris pH 8, 1 mM DTT, 1 mM NAD^+) to give a final volume of 50 μL. After incubation at 37°C for 30 min, the reaction was quenched by adding an equal volume of termination buffer (200 mM HCl, 320 mM glacial acetic acid, dissolved in methanol). The products were finally detected by HPLC-MS/MS.

ATP-citrate lyase enzyme activity assay

ADP-Glo Kinase Assay Kit (Promega, V6930) was used to determine the enzymatic activity of ACLY. The kinase reaction was performed in a final volume of 5 μL, initiated by adding 10 μM ATP, 100 μM CoA, a series of concentrations of citric acid (0, 6.25, 12.5, 25, 50 μM), and about 200 ng of ACLY WT (with or without 10 mM SB treatment)/K978A/K978bz to the reaction buffer (40 mM Tris pH 8.0, 10 mM $MgCl_2$, 5 mM DTT, 2% DMSO). After 30 min at 37°C, the kinase reaction was terminated by the addition of an equal volume of ADP-Glo reagent, and the remaining ATP was consumed. After 40 min of incubation at room temperature, 10 μL of the kinase assay reagent was added, which converts the ADP to ATP and detects the newly synthesized ATP using the coupled fluorescein enzyme/fluorescein reaction.

Protein extraction for proteomics

HepG2 cells treated with doxycycline for 48 h to induce SIRT2/SIRT3 knockdown were collected and washed twice with pre-cooled PBS, followed by the addition of lysis buffer (50 mM Tris-HCl pH 7.5, 150 mM sodium chloride, 1% Triton X-100, 1 mM EDTA, 1 mM DTT, containing protease inhibitors) and placed on ice for 30 min. The whole lysate was sonicated for an appropriate time and then centrifuged at high speed to remove fragments. The supernatant was collected and protein concentration was assayed using a BCA kit.

Trypsin digestion

Trichloroacetic acid (TCA) was slowly added to the above samples at a final concentration of 20% v/v and the samples were rest on ice for 30 min to allow complete precipitation of the proteins. The precipitate was then collected by centrifugation at 4,500 g for 5 min at 4°C, washed three times with pre-cooled acetone and dried on ice to remove residual acetone. The sample was then redissolved in 100 mM tetraethylammonium bromide. Trypsin was added at a ratio of 1:50 trypsin-to-protein mass ratio for overnight digestion at room temperature. The resulting peptides were treated with 5 mM dithiothreitol for 60 min at 37°C, followed by 11 mM iodoacetamide for 45 min at room temperature for reductive alkylation. Finally, the samples were desalted by C18 solid phase extraction column for subsequent mass spectrometry.

Pan Kbz-based post-translational modification enrichment

The peptide samples in NH_4HCO_3 solution were incubated with 30 μL of anti-pan Kbz beads at 4°C overnight. After incubation, the beads were washed three times with NETN buffer (50 mM Tris pH 8.0, 100 mM NaCl, 1 mM EDTA, 0.5% NP40), twice with ETN buffer (50 mM Tris pH 8.0, 100 mM NaCl, 1 mM EDTA), and once with water. The bound peptides were eluted from the beads with 0.1% trifluoroacetic acid and vacuum-dried.

HPLC-MS/MS analysis of Kbz

The sample analysis was carried out on an EASY-nLC 1200 UHPLC system (ThermoFisher Scientific) coupled with a Q Exactive HF-X mass spectrometer (ThermoFisher Scientific). Peptides were dissolved in 2.5 μL of solvent A (0.1% FA in water, v/v) and injected into a homemade packed capillary C18 column (20 cm length×75 μm ID, 1.9 μm particle size, Dr. Maisch GmbH, Germany). The quantitative proteome and immunoprecipitated Kbz samples were run in 180- and 120-min gradient, respectively, from 6% to 90% solvent B (A, 0.1% formic acid; B, 80% acetonitrile in 0.1% formic acid). Full mass scans were acquired with 350–1200 m/z at a mass resolution of 60,000. Ions with 2+, 3+, and 4+ charges were selected for MS/MS analysis. The 12 most intensive ions were fragmented with 28% normalized collision energy and tandem mass spectra were acquired with a mass resolution of 15,000. Dynamic exclusion was set to 30.0 s.

Protein sequence database searching

After LC-MS/MS acquisition, the raw files were qualitatively analyzed by MaxQuant software (version1.6.15.0) against the UniProt human database (20376 entries). Parameters set for quantitative proteomics identification include: Trypsin/P as the digestive enzyme; maximum missing cleavage of 2; minimum peptide length of 7; maximum FDR for peptides and proteins of 1%. Cysteine carbamidomethylation (+57.0215 Da) was established as a fixed modification. Methionine oxidation (+15.9949 Da) and acetylation of the N-terminus (+42.0106 Da) were established as variable modifications. Parameter setting of Kbz samples included lysine benzoylation (+104.0262 Da) as a variable modification. Other parameters were consistent with the proteome search. FDR thresholds for modification site were specified at 1%.

Bioinformatics analysis

The proteomics experiments were performed with three biological replicates, and MaxQuant LFQ algorithm was used for label-free quantification. To eliminate changes in Kbz peptide levels due to dynamic changes in protein levels, all Kbz site ratios were normalized by the quantified protein expression levels. GO and KEGG analyses were adopted with a hypergeometric test in the R clusterProfiler package.[59] The consensus sequence logo analysis was performed using iceLogo (v1.2).[60]

QUANTIFICATION AND STATISTICAL ANALYSIS

Experimental values are represented as mean ± SEM. $n = 3$ or 4, biologically independent sample. p value was assessed by one or two-tailed Student's t test. NS, not significant; *$p < 0.05$; **$p < 0.01$; ***$p < 0.001$.